Hindawi Publishing Corporation
Journal of Nanomaterials
Volume 2007, Article ID 16391, 8 pages
doi:10.1155/2007/16391

Research Article

Upconversion Properties of Nanocrystalline ZrO_2:Yb^{3+}, Er^{3+} Phosphors

Iko Hyppänen,[1] Jorma Hölsä,[1] Jouko Kankare,[1] Mika Lastusaari,[1] and Laura Pihlgren[1, 2, 3]

[1] *Department of Chemistry, University of Turku, FI-20014 Turku, Finland*
[2] *Department of Biotechnology, University of Turku, Tykistökatu 6, FI-20520 Turku, Finland*
[3] *Graduate School of Materials Research, Turku, Finland*

Received 30 October 2007; Accepted 26 November 2007

Recommended by Wiesław Stręk

Combustion and sol-gel methods were used to prepare the upconverting nanocrystalline ZrO_2:Yb^{3+},Er^{3+} phosphors. The crystal structure was studied by X-ray powder diffraction and the crystallite sizes were estimated with the Scherrer formula. Impurities and nanomaterials' thermal degradation were analyzed with FT-IR spectroscopy and thermal analysis, respectively. Upconversion luminescence and luminescence decays were studied with IR-laser excitation at 977 nm. All nanomaterials possessed the cubic ZrO_2 fluorite-type structure except for a small monoclinic impurity obtained with the sol-gel method. The conventional NO_3^- and OH^- impurities were observed for the combustion synthesis products. The ZrO_2:Yb_3,Er^{3+} nanomaterials showed red (630–710 nm) and green (510–570 nm) upconversion luminescence due to the $^4F_{9/2} \rightarrow {}^4I_{15/2}$ and $(^2H_{11/2}, {}^4S_{3/2}) \rightarrow {}^4I_{15/2}$ transitions of Er^{3+}, respectively. The products of the combustion synthesis exhibited the most intense luminescence intensity and showed considerable afterglow. It was concluded that excitation energy is partially trapped in the system and subsequently bleached thermally to the luminescent Er^{3+} center to yield "persistent upconversion".

1. INTRODUCTION

One of the most sophisticated and, at the same time, the most complex applications of lanthanide luminescence is in the medical diagnostics [1]. However, there are some major problems in the use of photoluminescence based on the UV excitation in immunoassays [2]. Human blood absorbs strongly UV radiation as well as the emission of the phosphor in the visible [3]. The observation of luminescence from the lanthanide labels is thus basically disadvantageous. One of the usual ways of overcoming this problem has been the application of long-lifetime lanthanide labels (e.g., those based on terbium and europium). However, the use of these Tb^{3+}-or Eu^{3+}-based lanthanide labels in the whole-blood immunoassays is still difficult because the Tb^{3+} luminescence (maximum emission at 545 nm) is in the same wavelength region as the blood absorption (<600 nm). The Eu^{3+} luminescence (maximum at 615–620 nm) is also slightly overlapping with the blood absorption. Persistent luminescence is a useful method to solve the blood emission problem if the UV excitation is used [4]. Persistent luminescence can be visible for several hours after the excitation has been ceased while the luminescence lifetime of the blood is in the ns range. Although most persistent luminescence materials emit in green or blue strongly absorbed by blood, some persistent luminescence emitters in the red are known (e.g., Mn^{2+}) [5, 6]. However, the Mn^{2+} ion needs a sensitizer (usually Eu^{2+}) which absorbs the exciting radiation.The upconversion luminescence where the absorption of two or more low-energy photons is followed by the emission of a photon of higher energy has witnessed numerous breakthroughs during the past decades. Upconverting phosphors have a variety of potential applications as lasers, displays, and inks for security printing (e.g., bank notes and bonds) [7–9]. In addition, another promising way to overcome the problems with the blood absorption is to use a long-wavelength excitation and benefit the upconversion luminescence [10]. There is practically no absorption by the whole-blood in the near IR region and it has no capability for upconversion in the excitation wavelength region of the conventional upconverting phosphor based on the Yb^{3+} (sensitizer) and Er^{3+} (activator) combination. It is also possible to find a red emitting ion (Er^{3+}).

For coupling to biological compounds, nanometer-sized upconverting phosphor particles are required. Moreover,

nanophosphors with high luminescent efficiency are vital in the development of novel homogeneous label technology for quantitative all-in-one whole-blood immunoassay which uses low-cost measurement devices [11].

In this work, nanocrystalline upconverting phosphors with zirconium oxide (zirconia, ZrO_2) as the host lattice were prepared. The local environment, the dopant concentration, and the distribution of active ions in the host material affect the upconversion efficiency [12, 13]. Taking into account these requirements (among others), zirconia offers a very appropriate medium for the preparation of highly luminescent materials because it is chemically and photochemically stable, and has a high refractive index (2.15–2.18) and a low phonon energy. The stretching frequency of the Zr–O-bond is about 470 cm^{-1}, which is much lower than for Al–O (870) or Si–O (1100) but higher than for Y–O (300–380 cm^{-1}) [12].

In the zirconia host, the lanthanide dopants possess multisite positions that improve the absorption efficiency and potentially enhance the resonant energy transfer from the sensitizer (Yb^{3+}) to the activator (Er^{3+}). The ZrO_2:Yb^{3+},Er^{3+} nanophosphors were obtained with several soft chemistry methods and the possible impurities were studied mainly with FT-IR spectroscopy. Materials' preparation and thermal degradation were studied with thermal analysis (TG, DTA). Crystal structures and phase purities were analyzed with X-ray powder diffraction (XPD). Upconversion luminescence and decays were obtained at room temperature with NIR excitation. A comparison was made between the luminescence intensities and the crystallite size, the crystal structure, as well as the impurities of the phosphors. Finally, a new phenomenon, persistent upconversion luminescence was introduced and discussed.

2. EXPERIMENTAL

The ZrO_2:Yb^{3+},Er^{3+} nanomaterials were prepared with the combustion [14] and sol-gel methods [15]. The synthesis affects the type and amount of impurities as well as the crystallite size, which in turn has a profound influence on the upconversion luminescence intensity. Accordingly, the method of preparation should be chosen carefully taking into account both the crystallite size as well as the intensity and color of luminescence of the nanomaterial. This may lead to quite difficult tradeoffs.

The precursor materials of ZrO_2:Yb^{3+},Er^{3+} prepared with the combustion synthesis were the aqueous solutions of zirconyl nitrate ($ZrO(NO_3)_2$) as well as ytterbium and erbium nitrates ($Yb(NO_3)_3$ and $Er(NO_3)_3$, resp.). The nominal concentrations of Yb^{3+} (99.9%) and Er^{3+} (99.99%) were ten and four mole-%, respectively, of the Zr^{IV} amount. Glycine (NH_2CH_2COOH), semicarbazide ($H_2NCONHNH_2 \cdot HCl$), urea ($(NH_2)_2CO$), citric acid ($HOC(COOH)(CH_2COOH)_2$), or 2-amino-2-methyl-1,3-propanediol (AMP, $(HOCH_2)_2C(NH_2)CH_3$) served as the fuel. Additional ammonium nitrate (NH_4NO_3) was used as an oxidizer with selected fuels. The combustion reaction was carried out in a glass reactor using a weak upward air flow. Some of the products were postannealed in air at 700°C for 1 hour if the material's crystallinity was poor.

The ZrO_2:Yb^{3+},Er^{3+} nanomaterials obtained with the sol-gel method had the zirconium-*n*-propoxide as a precursor to which the aqueous ytterbium and erbium nitrate solutions were added. After gelation, the materials were dried and annealed for 3 or 6 hours at 400°C and for 10 or 20 hours at 1000°C in static air in a ceramic crucible with a lid.

The FT-IR spectra between 400 and 4000 cm^{-1} were measured with a Mattson Instruments GALAXY 6030 spectrometer with a 4 cm^{-1} resolution. The materials were mixed with KBr and then pressed to transparent discs.

The TG and DTA curves between 25 and 1200°C were measured in flowing air (100 $cm^3\,min^{-1}$) with a TA instruments SDT 2960 Simultaneous DTA-TGA thermoanalyzer with a heating rate of 5°C min^{-1}. α-Al_2O_3 was used as both the reference and crucible material.

The crystal structure and phase purity of the ZrO_2:Yb^{3+},Er^{3+} nanomaterials were analyzed with the X-ray powder diffraction (XPD) measurements. The patterns were collected with a Huber 670 image plate (2θ range: 4–100°) Guinier-camera ($CuK\alpha_1$ radiation: 1.5406 Å).

The crystallite size of each ZrO_2:Yb^{3+},Er^{3+} nanomaterial was estimated from the diffraction data by using the Scherrer formula [16]

$$d = \frac{0.9 \times \lambda}{\beta \times \cos\theta}, \tag{1}$$

where, in this formula, d (m) is the mean crystallite size, λ (m) the X-ray wavelength, β (rad) the full width at half maximum (FWHM) of the [111] reflection ($2\theta = 30.2°$), and θ (°) half of the Bragg's angle (2θ). The reflection broadening due to the diffractometer setup was eliminated from the β_s-value by using a microcrystalline ZrO_2 reference (β_r):

$$\beta^2 = \beta_s^2 - \beta_r^2. \tag{2}$$

The upconversion luminescence spectra of the nanomaterials were measured at room temperature with an Ocean Optics PC2000-CCD spectrometer. The excitation (λ_{exc} = 977 nm) source was an HTOE FLMM-0980-711-1300m IR laser diode. The decay curves were measured with the same excitation source at 650 nm. The width of the excitation pulse was 1 millisecond. After each pulse there was a 9-millisecond delay before the next pulse. One measurement consisted of 1000 pulse-delay cycles.

3. RESULTS AND DISCUSSION

3.1. Material impurities

The FT-IR spectra of the ZrO_2:Yb^{3+},Er^{3+} nanomaterials revealed the presence of the conventional impurities (NO_3^-, OH^-) in the materials prepared by the combustion synthesis (see Figure 1). The amount of these impurities depended on the fuel used; the highest amount of impurities was observed when urea was used as a fuel. The organic compounds (fuels) were mainly decomposed to CO_2, H_2O, and NO_x, but it is possible that the nanomaterials contain also some carbon residue since the ZrO_2 nanomaterials prepared with the

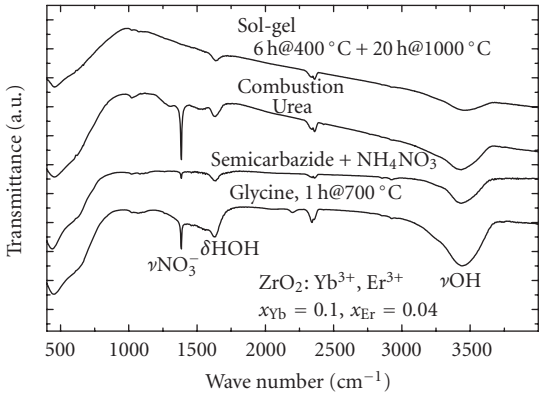

Figure 1: FT-IR spectra of selected ZrO_2:Yb^{3+},Er^{3+} nanomaterials prepared with the combustion synthesis.

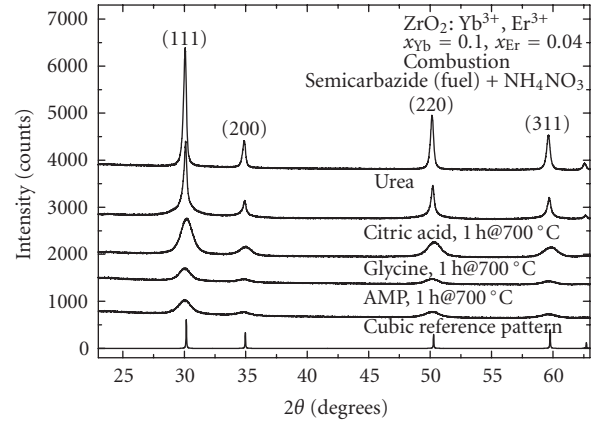

Figure 3: XPD patterns of selected ZrO_2:Yb^{3+},Er^{3+} nanomaterials prepared with the combustion synthesis.

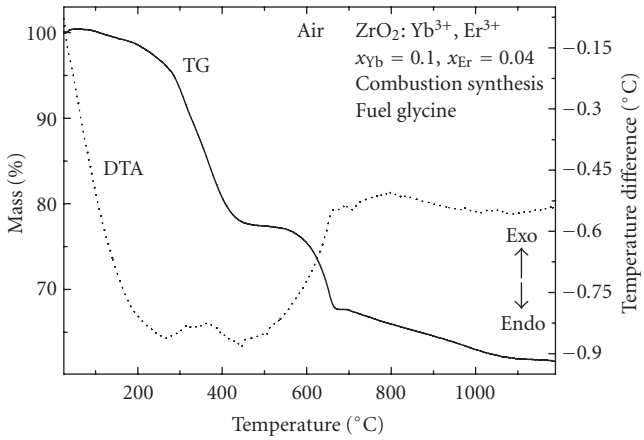

Figure 2: TG and DTA curves of the ZrO_2:Yb^{3+},Er^{3+} nanomaterial prepared by the combustion synthesis (glycine as the fuel).

combustion method were generally brown, whereas the body color of pure ZrO_2 is white. On the other hand, as to be discussed later in more detail, the substitution of Zr^{IV} with Yb^{3+}/Er^{3+} creates oxygen vacancies which may act as color centers, absorb in the visible, and cause the brownish color. No such impurities were observed in the ZrO_2:Yb^{3+},Er^{3+} nanomaterials prepared with the sol-gel method though it is evident that moisture was present in these materials. The amount of moisture (or OH^- groups) was greatly diminished by postannealing at 1100°C.

The stretching frequency of the Zr–O-bond is about 450 cm^{-1} (see Figure 1) which is in agreement with the literature value [12]. The Yb–O (or Er–O) vibrations could not be observed with the present experimental setup.

3.2. Thermal degradation

The TG curve of the ZrO_2:Yb^{3+},Er^{3+} nanomaterial, prepared with the combustion method, showed the decomposition of nitrates at 250–450°C (see Figure 2). No moisture was present because no low-temperature weight loss was observed below 200°C. With glycine used as the fuel, a further mass change was observed between 500 and 650°C. This change is due to the decomposition of zirconium oxycarbonates/oxynitrates which are surprisingly stable to high temperatures as are the corresponding rare earth oxycarbonates/oxynitrates [17, 18]. The exothermic signal in the DTA curve around 700°C can be related to the appearance of a crystalline phase of ZrO_2:Yb^{3+},Er^{3+} as indicated by the XPD patterns. The gradual weight loss at higher temperatures can be taken as an indication of evaporation of tightly bound species, for example, OH^- groups (as water). The presence of these impurities may have a nefarious effect on the luminescence performance of these nanomaterials.

The TG curve of the material prepared with the sol-gel method showed a practically constant weight. No signals were observed in the DTA curve either.

3.3. Crystal structure and crystallite sizes

The XPD measurements revealed that the structure of the ZrO_2:Yb^{3+},Er^{3+} nanomaterials was that of the typical cubic yttria stabilized zirconia (the cubic YSZ phase: space group Fm $\bar{3}$m, no. 225, $Z = 4$) [19]. The nanomaterials, prepared with the combustion synthesis (see Figure 3), were essentially pure, whereas small amounts of the monoclinic zirconia phase ($P2_1/a$, no. 14, $Z = 4$) [19] as an impurity was found in the materials prepared with the sol-gel method (see Figure 4). The presence of the monoclinic phase is probably due to the partial segregation of ZrO_2:Yb^{3+},Er^{3+} to the individual ZrO_2 and $(Yb,Er)_2O_3$ phases since very weak reflections belonging to R_2O_3 were noticed in the XPD patterns. The crystallite sizes estimated with the Scherrer equation [16] were 5–30 and ca. 50 nm for materials prepared with the combustion synthesis and the sol-gel method, respectively.

3.4. Upconversion luminescence

The excitation process for the upconversion emission of Er^{3+} ions (see Figure 5) under infrared excitation (λ_{exc} = 977 nm)

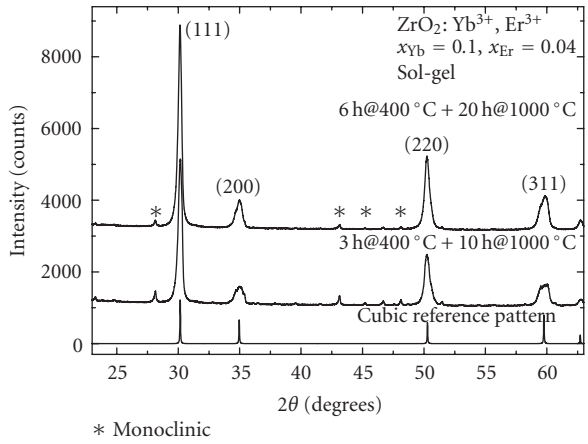

Figure 4: XPD patterns of selected ZrO_2:Yb^{3+},Er^{3+} nanomaterials prepared with the sol-gel method.

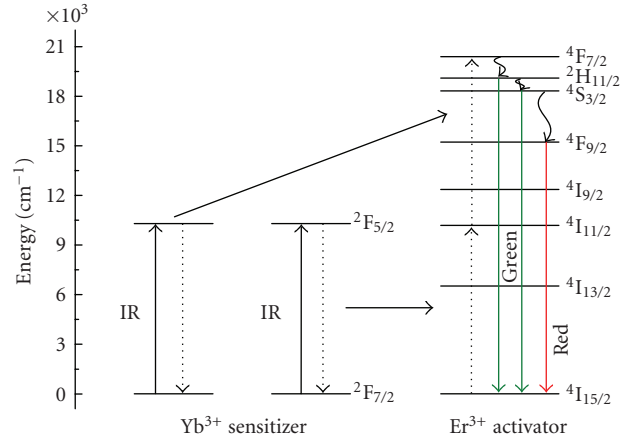

Figure 5: Schematic diagram of the Yb^{3+} sensitized Er^{3+} upconversion luminescence.

has been well established in the literature, for example, [20–22]. Though this mechanism is well known, in view of the phenomenon described later on, it is presented here as well. The first photon of near-infrared (NIR) radiation excites the Yb^{3+} ion to the sole excited $^2F_{5/2}$ level from which the excitation may relax radiatively back to the ground $^2F_{7/2}$ level. Taken into account the long radiative life time of the excited $^2F_{5/2}$ level (typically 1 millisecond), the Yb^{3+} ion may transfer well the excitation energy to an Er^{3+} ion with higher probability than decaying radiatively. The Er^{3+} ion is first promoted to the $^4I_{11/2}$ level, and further to $^4F_{7/2}$ due to absorption and energy transfer of another NIR photon. Then Er^{3+} decays rapidly and nonradiatively to the $^2H_{11/2}$, $^4S_{3/2}$ or $^4F_{9/2}$ (or lower) levels. The upconversion emission is customarily assigned to the following transitions: green emission in the 510–570 nm region to the ($^2H_{11/2}$, $^4S_{3/2}$)→$^4I_{15/2}$ transitions; and red emission in the 630–710 nm region to the $^4F_{9/2}$→$^4I_{15/2}$ transitions of the Er^{3+} ion. It should be noted that other pathways (including the initial ground-state absorption (GSA) and further excited-state absorption (ESA)) may be possible involving the Er^{3+} ions only, though their probabilities are low, partly due to the low Er^{3+} concentration.

In the ZrO_2 matrix, the luminescence transitions are rather broad and without evident crystal field fine structure. This observation is in agreement with the multisite positions occupied by the trivalent Yb^{3+} and Er^{3+} ions. This is due to the lack of any trivalent ion site in the ZrO_2 structure and the creation of oxide vacancies (Kröger-Vink notation: $V_O^{\bullet\bullet}$) results from the Yb^{3+} and Er^{3+} ions occupying the tetravalent Zr^{IV} site (Yb'_{Zr} or Er'_{Zr}) in the cubic fluorite type structure. At least three different sites with different point symmetries due to the different position of the oxide vacancies around the R^{3+} ion have been found for the ZrO_2:Y^{3+},Eu^{3+} system with the use of optical site selective excitation techniques [23] and EXAFS measurements [24]. Moreover, the inhomogeneous broadening of the Eu^{3+} emission lines was taken as an indication of a relaxation of the oxide sublattice towards the oxide vacancies creating a number of sites with rather similar point

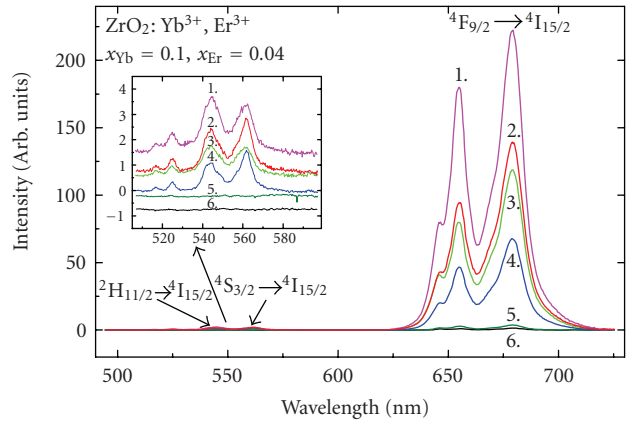

1. Semicarbazide + NH_4NO_3
2. Sol-gel, 6 h @ 400 °C + 20 h @ 1000 °C
3. Urea
4. Sol-gel, 3 h @ 400 °C + 10 h @ 1000 °C
5. AMP
6. Glycine, 1 h @ 700 °C

Figure 6: Upconversion luminescence spectra of selected ZrO_2:Yb^{3+},Er^{3+} nanomaterials.

symmetries. There is no doubt that similar charge compensation schemes are present in the ZrO_2:Yb^{3+},Er^{3+} nanomaterials because of the similar size of the Yb^{3+} and Y^{3+} dopants when compared to Zr^{IV}.

The highest luminescence intensity was obtained from the ZrO_2:Yb^{3+},Er^{3+} nanomaterials obtained with the combustion synthesis with semicarbazide used as the fuel (see Figure 6). This is due to the structurally pure (cubic) material, whereas the material prepared with the sol-gel method was a mixture of both the cubic and monoclinic forms. The difference between the luminescence intensities might also be due to the different surrounding microdomains of the Yb^{3+} and Er^{3+} ions, and due to other impurities.

The heating of the nanomaterial prepared with the combustion synthesis at 1100°C for 2 hours did not increase

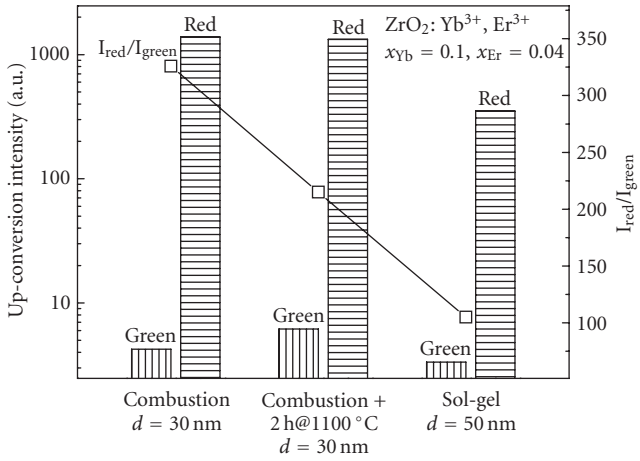

Figure 7: Upconversion luminescence intensities of selected ZrO_2:Yb^{3+},Er^{3+} nanomaterials.

the crystallite size. This might be due to a too low heatingtemperature and/or too short heating time. Because of the equal crystallite sizes, the luminescence intensities of the both materials prepared with the combustion synthesis were also quite equal.

The ZrO_2:Yb^{3+},Er^{3+} nanomaterials exhibit a very high I_{red}/I_{green} ratio (note the logarithmic y-scale in Figure 7) compared to other host materials (e.g., $NaYF_4$) [25]. This is due to the very low intensity of the green luminescence. In the ZrO_2 host, there are three main reasons for the weak green luminescence: the multiphonon relaxation, the cross-relaxation, and trapping of excitation energy by lattice defects. The prerequisites for efficient multiphonon relaxation are an energy level close below the luminescent level and/or high-energy phonon(s). The energy difference between the $^4S_{3/2}$ ($^2H_{11/2}$) levels yielding the green luminescence and the next lower level ($^4F_{9/2}$) is ca. 3000 cm^{-1} (ca. 3700). The Zr–O phonon energy is 470 cm^{-1} [12] and the Er–O energy is approximately the same. In pure materials, the multiphonon relaxation process is not probable because too many (six or seven) lattice phonons are needed to quench the green luminescence. However, when the crystallite size is smaller, there exist impurities (e.g., NO_3^-, OH^-) on the large surface area to facilitate the quenching. The surface itself may act as a quenching center too. The probability of the multiphonon relaxation is increased because the impurities have higher phonon energies (up to 1500 and 3500 cm^{-1} for NO_3^- and OH^-) and thus less phonons (one or two) are needed for quenching. Finally, the multiphonon relaxation of the green luminescence enhances the intensity of the red luminescence by populating the $^4F_{9/2}$ level.

The energy difference between the $^4F_{9/2}$ level yielding the red luminescent and the next lower $^4I_{9/2}$ level is also ca. 3000 cm^{-1}. The probability for the multiphonon relaxation of the red luminescence should be comparable to that of the green one. However, the red emission is much stronger and thus the multiphonon relaxation seems to be inefficient in this case. Finally, it should be noted that both the green and red luminescence of the ZrO_2:Yb^{3+},Er^{3+} nanomaterials are rather weak when compared to other host lattices studied (e.g., $NaYF_4$ and Y_2O_2S) [25]. The multiphonon relaxation processes can thus explain the weakness of the *total* but not the individual green luminescence alone.

The second process that may affect the luminescence intensities is cross-relaxation. There may be three possible cross-relaxation processes resulting in the quenching of the green luminescence. First of all, the quenching of the green emission from $^4S_{3/2}$ proceeds via the thermally activated $^2H_{11/2}$ level. The first process involves the $^2H_{11/2}\rightarrow{}^4I_{13/2}$ relaxation and the $^4I_{9/2} \leftarrow {}^4I_{15/2}$ excitation; the energy being ca. 12500 cm^{-1}. In the second possible cross-relaxation process, there are coupled the $^2H_{11/2}\rightarrow{}^4I_{9/2}$ relaxation and the $^4I_{13/2} \leftarrow {}^4I_{15/2}$ excitation [13]. The energy difference related to these processes is ca. 6700 cm^{-1}. It has been claimed that the two cross-relaxation mechanisms are experimentally indistinguishable [26]. The two cross-relaxation processes are competing with the green luminescence, with the multiphonon relaxation, with each other, and also with the trapping of energy. There are no known cross-relaxation processes for the red luminescence of Er^{3+} because of the lack of appropriate energy levels.

The third cross-relaxation process involves the higher excited $^4F_{7/2}$ level of Er^{3+} which relaxes to the red emitting $^4F_{9/2}$ level bypassing the green emitting levels [27]. The energy balance (ca. 5000 cm^{-1}) is conserved by the excitation of Er^{3+} to the $^4F_{9/2}$ level from the $^4I_{11/2}$ level which is populated due to the NIR laser pumping. Indeed, this process would favor the red emission.

The cross-relaxation processes of Er^{3+} is naturally favored by the rather high erbium concentration in the ZrO_2:Yb^{3+},Er^{3+} nanomaterials (nominally four mole-%) because then the erbium ions can locate near each other. As a special feature in the zirconia host, the Er^{3+} ions can form pairs with the aid of the oxide vacancy, that is, $Er^{3+}-V_O^{\bullet\bullet}-Er^{3+}$ (cf. above). In addition to the intraion cross-relaxation processes, the interion ones can thus occur more easily between the Er^{3+} ions and decrease the intensity of the green luminescence.

The very weak green luminescence can thus be explained with both the multiphonon and the cross-relaxation processes but the strong red luminescence only with one of the cross-relaxation processes. However, in order to judge the relative probabilities of these processes, much more detailed spectroscopic work is needed. At the moment, this is out of the scope of the present work.

The energy trapping caused by the oxygen vacancies (cf. the discussion about the color centers above and Section 3.5) is also a competing process with the multiphonon and cross-relaxation processes. The total luminescence intensity can be quenched due to the absorption of the excitation energy but it may also affect the relative intensities of the green and red luminescence.

3.5. Upconversion luminescence decay

The study of the dynamics of the Er^{3+} red upconversion luminescence from the ZrO_2:Yb^{3+},Er^{3+} nanomaterials was

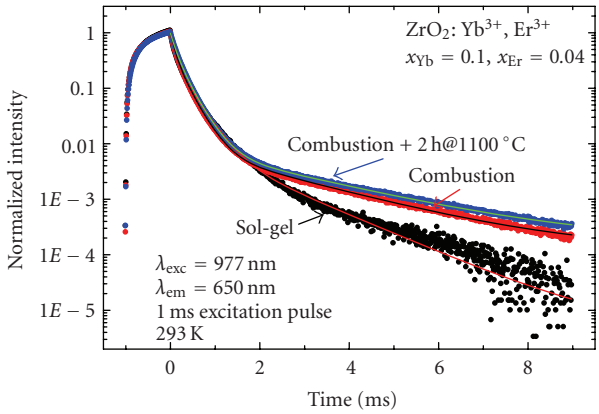

Figure 8: Upconversion luminescence decay curves of selected ZrO_2:Yb^{3+},Er^{3+} nanomaterials.

decided to be carried out in two phases: first the feeding processes taking place before (or simultaneously to) the Er^{3+} luminescence; then the decay characteristics of the proper luminescence were examined in detail. It is evident with the first glance at Figure 8, however, that the preluminescence period was too complex and contained too few pieces of information to be exploited to yield reliable results. It should, nevertheless, be noted that the upconversion luminescence feeding time is very long (more than 1 millisecond). It can be deduced in a semiquantitative manner that the Yb^{3+} to Er^{3+} energy transfer is not exceedingly efficient since the other processes involved in the upconversion (absorption by Yb^{3+} (and Er^{3+}) and relaxation from the higher Er^{3+} levels to the emitting $^4F_{9/2}$ level) should take only a fraction of time when compared to the customary one-millisecond decay time of Yb^{3+}. The probability of the Yb^{3+}–Er^{3+} energy transfer can be deduced to be of the same order of magnitude as the emission from Yb^{3+}. This is supported by the luminescence feeding curve which barely achieves the saturation point during the one-millisecond excitation pulse. The Yb^{3+}-to-Er^{3+} energy transfer seems to be the rate determining step in the excitation process and thus the time to reach the saturation can give some information about the probability of the energy transfer process.

The second part of the decay kinetics proved to be as complex as the first part. However, due to a more expanded time scale, some quantitative measurements and calculations could be accomplished. The fitting of the red upconversion luminescence decay curves, clearly multiexponential or even more complicated, could be carried out to individual exponential components in the linear part of the curves immediately after the influence of the feeding processes had ceased. The results of these calculations showed that there are at least two different luminescence lifetimes in a range from ca. 100 to ca. 300 microseconds. These values are quite typical for the regular red Er^{3+} luminescence [27] and the number of different decay times is consistent with the multisite positions occupied by the Er^{3+} ion. The decay curves show also that there is no significant difference between the different preparation methods when the shorter lifetimes are considered. Nevertheless, there is a significant difference in the *long* lifetimes of the nanomaterials prepared with different methods. For the ZrO_2:Yb^{3+},Er^{3+} nanomaterials prepared with the com-bustion synthesis (and subsequently heated at 1100°C for 2 hours), there was observed severe afterglow. The total length of this afterglow could not be measured because of the ex-perimental setup but it will definitely extend to several tens of milliseconds. This afterglow was hardly observed by the naked eye adapted to darkness and thus does not fulfill the requirements of the term "persistent luminescence" in the strictest meaning of the definition (light observed at the il-lumination level of 0.32 mcd m^{-2}). However, it should be noted that the ZrO_2:Yb^{3+},Er^{3+} nanomaterials for which this afterglow was observed were not optimized for this effects, for example, by adding agents to create lattice defects. The intense and long upconversion luminescence indicates that there occurs trapping of the excitation energy in the system followed by thermal bleaching of this energy and feeding to a luminescence center. In that sense, this emission can be called as "persistent upconversion luminescence".

As for the mechanism(s) of this persistent upconversion, there are two main possibilities: the trapping of the excitation energy can take place either after the absorption by Yb^{3+} (the sensitizer) or after the final excitation processes by Er^{3+} (the activator). The slightly more probable choice is the energy storage in the vicinity of Yb^{3+} since the decay time of Yb^{3+} is 3 to 10 times that of Er^{3+}. As a further proof to the existence of persistent luminescence for either Yb^{3+}- or Er^{3+}-doped materials, one can find experimental data for (strong) afterglow from Yb^{3+}-doped garnets [28, 29], Er^{3+}- doped silicon, and oxysulfides [28, 30, 31]. It can be thus as-sumed, though not yet proved, that the persistent upcon-version in the ZrO_2:Yb^{3+},Er^{3+} nanomaterials is possible. The resolution of the exact mechanism(s) requires further work, however.

Even without further studies, it is clear that there are vacancies (together with other impurities, e.g., OH^- groups) present in the ZrO_2:Yb^{3+},Er^{3+} nanomaterials both due to the size and charge mismatch between the trivalent Yb^{3+} (and Er^{3+}) and the tetravalent Zr^{IV} ions as well as to the soft chemistry preparation methods used. Similar defects are known to store energy in the persistent luminescence materials (such as Eu^{2+}-doped alkaline earth aluminates and silicates) [32] as well as in the photostimulated materials (such as Eu^{2+}-doped BaF(Cl,Br)) [33]. In the case of the ZrO_2:Yb^{3+},Er^{3+} nanomaterials, the depths of these traps are compatible with the thermal energy (kT) at room temperature and thus the feeding from the traps can occur.

The probability of trapping the excitation energy can be assumed to be a few orders of magnitude lower than the energy transfer to Er^{3+} or the emission of the Yb^{3+} ion. This can, however, be improved by careful engineering of these materials, as has been done with the alkaline earth aluminates and silicates. It can be assumed that the major advantages of combining the persistent luminescence and IR upconversion are that it can lead to efficient immunoassay materials.

4. CONCLUSIONS

The combustion method was found to be an efficient way to prepare the nanocrystalline upconverting ZrO_2:Yb^{3+},Er^{3+} luminescence materials with the cubic ZrO_2 structure. The sol-gel method yielded a mixed product with slightly larger crystallite sizes, however. All materials showed rather efficient red upconversion luminescence with broad features due to multiple Er^{3+} sites originating from different charge compensation schemes because of aliovalent substitution of Zr^{IV} with R^{3+}. As a result of the structural purity, the combustion route yielded products with the highest luminescence intensity. The red/green intensity ratio was found to increase with the decreasing crystallite size due to the weakening of the green luminescence. This may be due to a very complex relaxation process involving the multiphonon, cross-relaxation, as well as energy trapping caused by lattice defects. Only one of several cross-relaxation processes can explain at the same time the weak green and strong red luminescence, however. This process must thus be considered as the dominating relaxation process of the green luminescence.

The luminescence decay characteristics with at least two different lifetimes in the range typical of red Er^{3+} luminescence agreed with the multisite nature of the ZrO_2 lattice. The materials obtained with different methods showed considerable differences in the longer lifetimes. Moreover, severe afterglow, that is, persistent upconversion luminescence, was observed for the products of the combustion route indicating the inherent energy storage capability of the ZrO_2:Yb^{3+},Er^{3+} materials.

For efficient use in bioassays, more work is needed to yield nanomaterials with smaller and more uniform crystallite sizes. Surface modifications need to be studied to allow for the dispersion in aqueous solutions. On the other hand, further work must be carried out to optimize the persistent luminescence of the ZrO_2:Yb^{3+},Er^{3+} nanomaterials to allow for their use as efficient immunoassay nanomaterials combining the advantages of both upconversion and persistent luminescence.

ACKNOWLEDGMENTS

Financial supports from the Finnish Funding Agency for Technology and Innovation (Tekes) and the Graduate School of Materials Research (Turku, Finland) for L. Pihlgren and from the Graduate School of Chemical Sensors and Microanalytical Systems (Espoo, Finland) for I. Hyppänen are gratefully acknowledged.

REFERENCES

[1] S. N. Misra, M. A. Gagnani, I. Devi, and R. S. Shukla, "Biological and clinical aspects of lanthanide coordination compounds," *Bioinorganic Chemistry and Applications*, vol. 2, no. 3-4, pp. 155–192, 2004.

[2] G. Mathis, "Rare earth cryptates and homogeneous fluoroimmunoassays with human sera," *Clinical Chemistry*, vol. 39, no. 9, pp. 1953–1959, 1993.

[3] W. G. Zijlstra, A. Buursma, and W. P. Meeuwsen-van der Roest, "Absorption spectra of human fetal and adult oxyhemoglobin, de-oxyhemoglobin, carboxyhemoglobin, and methemoglobin," *Clinical Chemistry*, vol. 37, no. 9, pp. 1633–1638, 1991.

[4] Q. L. de Chermont, C. Chanéac, J. Seguin, et al., "Nanoprobes with near-infrared persistent luminescence for in vivo imaging," *Proceedings of the National Academy of Sciences of the United States of America*, vol. 104, pp. 9266–9277, 2007.

[5] T. Aitasalo, A. Hietikko, D. Hreniak, et al., "Structure and luminescence of $BaMg_2Si_2O_7$:Eu^{2+},Mn^{2+}($,R^{3+}$)," to appear in *Journal of Alloys and Compounds*.

[6] X.-J. Wang, D. Jia, and W. M. Yen, "Mn^{2+} activated green, yellow, and red long persistent phosphors," *Journal of Luminescence*, vol. 102-103, pp. 34–37, 2003.

[7] S. G. Grubb, K. W. Bennett, R. S. Cannon, and W. F. Humer, "CW room-temperature blue up-conversion fibre laser," *Electronics Letters*, vol. 28, no. 13, pp. 1243–1244, 1992.

[8] E. Downing, L. Hesselink, J. Ralston, and R. Macfarlane, "A three-color, solidstate, three-dimensional display," *Science*, vol. 273, no. 5279, pp. 1185–1189, 1996.

[9] R. Gutmann, B. Ahlers, F. Kappe, R. Paugstadt, and A. Franz-Burgholz, US Patent no. 6,234,537, 2001.

[10] E. Soini, N. J. Meltola, A. E. Soini, J. Soukka, J. T. Soini, and P. E. Hänninen, "Two photon fluorescence excitation in detection of biomolecules," *Biochemical Society Transactions*, vol. 28, pp. 70–74, 2000.

[11] T. Soukka, K. Kuningas, T. Rantanen, V. Haaslahti, and T. Lövgren, "Photochemical characterization of up-converting inorganic lanthanide phosphors as potential labels," *Journal of Fluorescence*, vol. 15, no. 4, pp. 513–528, 2005.

[12] A. Patra, C. S. Friend, R. Kapoor, and P. N. Prasad, "Upconversion in Er^{3+}:ZrO_2 nanocrystals," *Journal of Physical Chemistry B*, vol. 106, no. 8, pp. 1909–1912, 2002.

[13] A. Patra, C. S. Friend, R. Kapoor, and P. N. Prasad, "Effect of crystal nature on up-conversion luminescence in Er^{3+}:ZrO_2 nanocrystals," *Applied Physics Letters*, vol. 83, no. 2, pp. 284–286, 2003.

[14] F. Vetrone, J.-C. Boyer, J. A. Capobianco, A. Speghini, and M. Bettinelli, "Significance of Yb^{3+} concentration on the up-conversion mechanisms in codoped Y_2O_3:Er^{3+},Yb^{3+} nanocrystals," *Journal of Applied Physics*, vol. 96, no. 1, pp. 661–667, 2004.

[15] L. A. Díaz-Torres, E. De la Rosa-Cruz, P. Salas, and C. Angeles-Chavez, "Concentration enhanced red up-conversion in nanocrystalline ZrO_2: Er under IR excitation," *Journal of Physics D*, vol. 37, no. 18, pp. 2489–2495, 2004.

[16] H. P. Klug and L. E. Alexander, *X-Ray Powder Diffraction Procedures*, Wiley, New York, NY, USA, 1959.

[17] M. Karppinen, P. Kyläkoski, L. Niinistö, and C. Rodellas, "Thermal decomposition as a preparative route to anhydrous rare earth nitrates," *Journal of Thermal Analysis*, vol. 35, no. 2, pp. 347–353, 1989.

[18] J. Hölsä and T. Turkki, "Preparation, thermal stability and luminescence properties of selected rare earth oxycarbonates," *Thermochimica Acta*, vol. 190, pp. 335–343, 1991.

[19] PCPDFWIN v. 1.30, "Powder diffraction file," International Centre for Diffraction Data, entries 27-0997 (cubic ZrO_2) and 37-1484 (monoclinic ZrO_2), 1997.

[20] Y. Mita, "Infrared up-conversion phosphors," in *Phosphor Handbook*, S. Shionoya and W. M. Yen, Eds., pp. 643–650, CRC Press, Boca Raton, Fla, USA, 1999.

[21] F. Auzel, "Up-conversion in rare-earth-doped systems: past, present and future," in *XI Feofilov Symposium on Spectroscopy*

of Crystals Activated by Rare-Earth and Transition Metal Ions, vol. 4766 of *Proceedings of SPIE*, pp. 179–190, Kazan, Russia, September 2001.

[22] F. Auzel, "Up-conversion and anti-Stokes processes with f and d ions in solids," *Chemical Reviews*, vol. 104, no. 1, pp. 139–173, 2004.

[23] J. Dexpert-Ghys, M. Faucher, and P. Caro, "Site selective spectroscopy and structural analysis of yttria-doped zirconia," *Journal of Solid State Chemistry*, vol. 54, no. 2, pp. 179–192, 1984.

[24] M. H. Tuilier, J. Dexpert-Ghys, H. Dexpert, and P. Lagarde, "X-ray absorption study of the ZrO_2-Y_2O_3 system," *Journal of Solid State Chemistry*, vol. 69, no. 1, pp. 153–161, 1987.

[25] I. Hyppänen, J. Hölsä, J. Kankare, M. Lastusaari, and L. Pihlgren, Unpublished results.

[26] M. Campbell and C. D. Flint, "Back transfer in the $^4S_{3/2}$ state of $Cs_2NaEr_xY_{1-x}Cl_6$ extension of the shell model," *Spectrochimica Acta A*, vol. 54, no. 11, pp. 1583–1591, 1998.

[27] F. Vetrone, J.-C. Boyer, J. A. Capobianco, A. Speghini, and M. Bettinelli, "Concentration-dependent near-infrared to visible up-conversion in nanocrystalline and bulk Y_2O_3:Er^{3+}," *Chemistry of Materials*, vol. 15, no. 14, pp. 2737–2743, 2003.

[28] M. Forcales, T. Gregorkiewicz, I. V. Bradley, and J.-P. R. Wells, "Afterglow effect in photoluminescence of Si:Er," *Physical Review B*, vol. 65, no. 19, Article ID 195208, 8 pages, 2002.

[29] J. W. Zhang, Y.-L. Liu, and S.-Q. Man, "Afterglow phenomenon in erbium and titanium codoped Gd_2O_2S phosphors," *Journal of Luminescence*, vol. 117, no. 2, pp. 141–146, 2006.

[30] N. Guerassimova, N. Garnier, C. Dujardin, A. G. Petrosyan, and C. Pédrini, "X-ray-excited charge transfer luminescence in YAG:Yb and YbAG," *Journal of Luminescence*, vol. 94-95, pp. 11–14, 2001.

[31] N. Guerassimova, N. Garnier, C. Dujardin, A. G. Petrosyan, and C. Pédrini, "X-ray excited charge transfer luminescence of ytterbium-containing aluminium garnets," *Chemical Physics Letters*, vol. 339, no. 3-4, pp. 197–202, 2001.

[32] T. Aitasalo, J. Hölsä, H. Jungner, M. Lastusaari, and J. Niittykoski, "Thermoluminescence study of persistent luminescence materials: Eu^{2+}- and R^{3+}-doped calcium aluminates, $CaAl_2O_4$:Eu^{2+},R^{3+}," *Journal of Physical Chemistry B*, vol. 110, no. 10, pp. 4589–4598, 2006.

[33] S. Schweizer, "Physics and current understanding of X-ray storage phosphors," *Physica Status Solidi (a)*, vol. 187, no. 2, pp. 335–393, 2001.